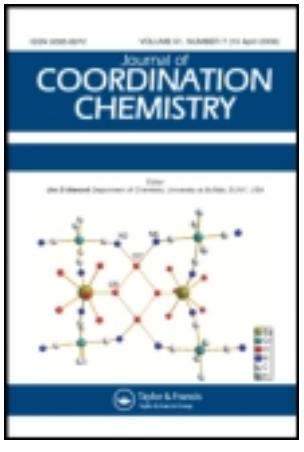

Journal of Coordination Chemistry
Publication details, including instructions for authors and subscription information:
http://www.tandfonline.com/loi/gcoo20

Designing nickel phthalocyanine periphery by alkyl chain via [1,3,4]-oxadiazole

M.N.K. Harish [a] , J. Keshavayya [a] , K.R. Venugopala Reddy [b] & H.R. Mallikarjuna [c]

[a] Department of Chemistry , School of Chemical Sciences, Jnana Sahyadri, Kuvempu University , Shankaraghatta - 577 451, Shimoga, Karnataka, India

[b] Department of Industrial Chemistry , Sahyadri Science College , Shimoga - 577 203, Karnataka, India

[c] Department of Chemistry , Rajiv Institute of Technology , Hassan - 573 201, Karnataka, India

Published online: 13 Jun 2011.

To cite this article: M.N.K. Harish , J. Keshavayya , K.R. Venugopala Reddy & H.R. Mallikarjuna (2011) Designing nickel phthalocyanine periphery by alkyl chain via [1,3,4]-oxadiazole, Journal of Coordination Chemistry, 64:12, 2075-2087, DOI: 10.1080/00958972.2011.588705

To link to this article: http://dx.doi.org/10.1080/00958972.2011.588705

Journal of Coordination Chemistry
Vol. 64, No. 12, 20 June 2011, 2075–2087

Taylor & Francis
Taylor & Francis Group

Designing nickel phthalocyanine periphery by alkyl chain *via* [1,3,4]-oxadiazole

M.N.K. HARISH†, J. KESHAVAYYA*†, K.R. VENUGOPALA REDDY‡ and H.R. MALLIKARJUNA§

†Department of Chemistry, School of Chemical Sciences, Jnana Sahyadri, Kuvempu University, Shankaraghatta – 577 451, Shimoga, Karnataka, India
‡Department of Industrial Chemistry, Sahyadri Science College, Shimoga – 577 203, Karnataka, India
§Department of Chemistry, Rajiv Institute of Technology, Hassan – 573 201, Karnataka, India

(*Received 11 February 2011; in final form 12 April 2011*)

Nickel phthalocyanine (**NiPc, 1**) periphery has been decorated by alkyl chains of varying chain length *via* [1,3,4]-oxadiazole moiety (**NiPcs 3a–3f**). All the newly synthesized compounds **NiPcs 3a–3d** have been completely characterized by elemental analysis, FT-IR, solid-state UV-Vis, and solid-state ^{13}C NMR spectroscopy, in addition to X-ray diffraction, scanning electron microscopy, and thermal analysis. The effect of chain length in the NiPc periphery on electronic absorption and DC electrical conductivity has been investigated.

Keywords: Phthalocyanine; [1,3,4]-Oxadiazole; Alkyl; Solid-state electronic absorption spectra; Solid-state ^{13}C NMR; DC electrical conductivity

1. Introduction

The richness of physical and chemical properties of phthalocyanines (Pcs) and their numerous potential applications in emerging technologies, including energy conservation, molecular electronics, and sensors, gave powerful stimulus to the development and synthesis of structurally diverse Pc molecules [1–11]. The advantageous properties of alkyl substituents on Pcs have gained considerable attention in the field of materials science. The discovery of mesogenic Pcs in 1982 [12] have attracted much attention of researchers active in the field, because of their fascinating optical and electronic properties [13–16] which make them potential candidates for optoelectronic devices. A variety of alkylated Pcs have been prepared by varying the number, type, length, and position of the flexible substituents, as well as by the incorporation of a metal ion in the cavity of the Pc molecule [17–26].

The need for new chromophores with intense absorptions at the far red end or the near infrared (IR) region of the electromagnetic spectrum is evident from the recent

*Corresponding author. Email: jkeshavayya@gmail.com

ISSN 0095-8972 print/ISSN 1029-0389 online © 2011 Taylor & Francis
DOI: 10.1080/00958972.2011.588705

developments in materials science and medicinal chemistry. In our previous work on 2,9,16,23-tetra aryl-[1,3,4]-oxadiazole-substituted NiPc, we demonstrated the synthesis, characterization, electronic, and DC electrical conductivity [27]. This study is a continuation of our earlier work on alkyl [1,3,4]-oxadiazole-substituted Nipcs.

Oxadiazole-bearing organic compounds have efficient electron-transporting and hole-blocking properties with high thermal stability [28–33]. The [1,3,4]-oxadiazole building block is an attractive unit, because it is a good electron-withdrawing group, relatively stable, and is easy to build as part of a π-conjugated system. Discotic oxadiazoles, with columnar mesophases, were proposed for applications in organic electronics [34].

No reports are available on peripheral alkyl oxadiazole-substituted metallo-Pcs (MPcs). These findings increase the value of the mentioned synthetic strategy to explore the potential of alkyl oxadiazole-substituted Pcs. This article demonstrates the properties of new [1,3,4]-oxadiazole-substituted Nipcs bearing alkyl chains of varying length (figure 1). In particular, we have attempted to find DC conductivity behavior, spectral response, and stability of these compounds as a function of alkyl chain length.

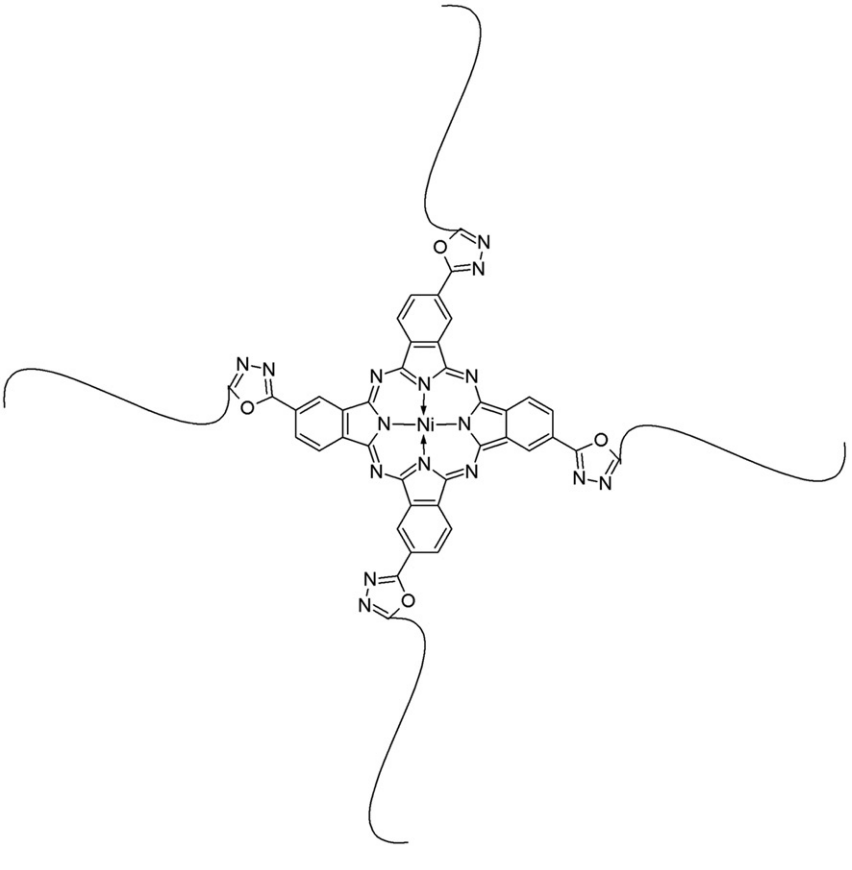

Figure 1. 2,9,16,23-tetra alkyl-[1,3,4]-oxadiazole-substituted NiPc.

2. Experimental

2.1. *Materials*

1,2,4-Benzene tricarboxylic anhydride was purchased from Aldrich; other chemicals were obtained from Merck (India) and used without purification. Tetracarboxy nickel phthalocyanine (**TCPNi**) [35] was prepared according to the described procedure.

2.2. *Instrumentation*

Elemental analyses were obtained from a 1106 Carlo-Erba instrument. IR spectra were recorded on a FT-IR 8400s SHIMADZU spectrometer in KBr pellets. Solid-state electronic absorption spectra were recorded on a PERKIN-ELMER UV-Vis spectrometer, model UV/VIS-35. Solid-state ^{13}C NMR spectra were recorded on a BRUKER DSX-300 solid-state NMR spectrometer with magnetic field of 7.04 T and carbon frequency of 75.47 MHz (internal standard: glycine). Mass spectra were recorded with a LC-MSD-trap-XCTplus mass spectrometer. Powdered X-ray diffraction (XRD) measurements were carried out on a Bruker D8 AVANCE X-ray diffractometer. DC electrical conductivity measurements were carried out by the two probe method using a KEITHLEY source meter (Model-2400). A calibrated chromel–alumel thermocouple was used to measure the temperature of the sample. For DC electrical conductivity measurements, powder samples were pressed uniaxially into a pellet of thickness $\approx$2 mm and of diameter 10 mm by applying a pressure of 100 Mpa for 3 min. The pellets were sintered at 100°C for 3 h to eliminate trapped oxygen and to get thermal stability. Fine quality silver paint was applied on both sides of the pellets for good electrical contacts. The pellet was sandwiched tightly between two steel rods in a sample holder with the help of screws and kept in a cell. Then the cell was placed in a muffle furnace. A suitable constant and low voltage (5 V) was applied across the pellet and the corresponding current through the sample was measured from 300 to 500 K. The conductivity readings were recorded during the heating cycle.

2.3. *General method for the synthesis of alkyl carboxylic acid hydrazides*

To a stirred solution of **2a–2f** (0.01 mol) in dry methanol (15 mL) at 0°C, thionyl chloride (0.03 mol) was added dropwise. After complete addition the mixture was brought to room temperature and refluxed for 5 h. The solvent was removed in vacuum and the oily product thus obtained was treated with saturated sodium bicarbonate solution and extracted in diethyl ether. The ether layer was concentrated to get the methyl ester of the corresponding alkyl carboxylic acids. To a stirred solution of methyl ester alkyl carboxylic acid (0.01 mol) in methanol (15 mL), hydrazine hydrate 99% (0.04 mol) was added dropwise. After complete addition of hydrazine hydrate the reaction mixture was refluxed for 8–12 h. The reaction mixture was cooled to room temperature and treated with brine solution; the solid product was collected, washed repeatedly with brine solution, and recrystallized from ethanol to get pure alkyl acid hydrazide **2g–2l**.

2.3.1. *n*-Caprylic acid hydrazide (2g). Yield: 68% (1.0 g); IR [(KBr) ν_{max}/cm^{-1}]: 3315 (–NH str.), 3179 ($–NH_2$ str.), 2922 (–C–H str.), 1630 (–C = O str.); ^1H NMR (DMSO-d_6, ppm): 8.6 (br, s, –NH, 1H), 4.12 (s, $–NH_2$, 2H), 1.99–1.94 (br, m, –CH, 2H), 1.45 (br, –CH, 2H), 1.25–1.02 (br, m, –CH, 8H), 0.84–0.82 (br, m, $–CH_3$, 3H); ^{13}C NMR (DMSO-d_6, ppm): 160 (–C = O), 19.4, 14, 13.3 (–CH); LCMS: $m/z = 159.8$ (M + 1).

2.3.2. *n*-Capric acid hydrazide (2h). Yield: 70% (1.3 g); IR [(KBr) ν_{max}/cm^{-1}]: 3315 (–NH str.), 3179 ($–NH_2$ str.), 2920 (–C–H str.), 1629 (–C = O str.); ^1H NMR (DMSO-d_6, ppm): 8.87 (br, s, –NH, 1H), 4.1 (s, $–NH_2$, 2H), 1.99–1.94 (br, m, –CH, 2H), 1.44 (br, –CH, 2H), 1.2 (br, –CH, 12H), 0.83–0.81 (br, m, $–CH_3$, 3H); ^{13}C NMR (DMSO-d_6, ppm): 160 (–C = O), 20.1, 14, 13.2 (–CH); LCMS: $m/z = 187.8$ (M + 1).

2.3.3. Lauric acid hydrazide (2i). Yield: 72% (1.5 g); IR [(KBr) ν_{max}/cm^{-1}]: 3316 (–NH str.), 3180 ($–NH_2$ str.), 2919 (–C–H str.), 1629 (–C = O str.); ^1H NMR (DMSO-d_6, ppm): 8.89 (br, s, –NH, 1 H), 4.2 (s, $–NH_2$, 2H), 1.99–1.94 (br, m, –CH, 2H), 1.45 (br, –CH, 2H), 1.22–1.13 (br, m, –CH, 16H), 0.84–0.81 (br, m, $–CH_3$, 3H); ^{13}C NMR (DMSO-d_6, ppm): 159 (–C = O), 20.1, 13.9, 13.3 (–CH); LCMS: $m/z = 215.7$ (M + 1).

2.3.4. Myristic acid hydrazide (2j). Yield: 70% (1.6 g); IR [(KBr) ν_{max}/cm^{-1}]: 3314 (–NH str.), 3179 ($–NH_2$ str.), 2921(–C–H str.), 1630 (–C = O str.); ^1H NMR (DMSO-d_6, ppm): 8.87 (br, s, –NH, 1 H), 4.1 (s, $–NH_2$, 2H), 1.99–1.94 (br, m, –CH, 2H), 1.45 (br, –CH, 2H), 1.28–1.14 (br, –CH, 20H), 0.83–0.81 (br, m, $–CH_3$, 3H); ^{13}C NMR (DMSO-d_6, ppm): 160 (–C = O), 20.1, 14, 13.2 (–CH); LCMS: $m/z = 243.3$ (M + 1).

2.3.5. Palmitic acid hydrazide (2k). Yield: 56% (1.5 g); IR [(KBr) ν_{max}/cm^{-1}]: 3318 (–NH str.), 3180 ($–NH_2$ str.), 2919 (–C–H str.), 1630 (–C = O str.); ^1H NMR (DMSO-d_6, ppm): 8.89 (br, s, –NH, 1H), 4.2 (s, $–NH_2$, 2H), 1.99–1.94 (br, m, –CH, 2H), 1.44 (br, –CH, 2H), 1.23–1.14 (br, –CH, 24H), 0.83–0.81 (br, m, $–CH_3$, 3H); ^{13}C NMR (DMSO-d_6, ppm): 159 (–C = O), 20.2, 14.1, 13.3 (–CH); LCMS: $m/z = 271.6$ (M + 1).

2.3.6. Stearic acid hydrazide (2l). Yield: 49% (1.4 g); IR [(KBr) ν_{max}/cm^{-1}]: 3318 (–NH str.), 3185 ($–NH_2$ str.), 2919 (–C–H str.), 1629 (–C = O str.); ^1H NMR (DMSO-d_6, ppm): 8.87 (br, s, –NH, 1H), 4.1 (s, $–NH_2$, 2H), 1.99–1.94 (br, m, –CH, 2H), 1.44 (br, –CH, 2H), 1.2 (br, –CH, 28H), 0.83–0.81 (br, m, $–CH_3$, 3H); ^{13}C NMR (DMSO-d_6, ppm): 159 (–C = O), 20.1, 14, 13.3 (–CH); LCMS: $m/z = 299.4$ (M + 1).

2.4. *General method for the synthesis of 2,9,16,23-tetra alkyl 1,3, 4-oxadiazole-substituted Nipc*

Nickel tetracarboxy phthalocyanine (**TCPNi**) (0.001 mol) and aromatic carboxylic acid hydrazides **2g–2l** (0.006 mol) were stirred into preheated polyphosphoric acid (100 g) containing 10 g of P_2O_5 at 100°C for 1 h, then heated at 120°C for 10 h and again heated at 150°C for 12 h. The reaction mixture was allowed to cool to 100°C and was quenched

with ice cold water and filtered. The product obtained was repeatedly treated with 0.1 N sodium hydroxide solution followed by water, hot acetic acid, 10% sodium bicarbonate solution, water, and acetone to get **3a–3f**.

2.4.1. 2,9,16,23-tetra-{2-heptyl-[1,3,4]oxadiazole}-nickelphthalocyanine (3a). Yield: 90% (1.11 g); Anal. Calcd for $C_{68}H_{72}N_{16}NiO_4$: C(66.07%); H(5.87%); N(18.13%). Found: C(65.10%); H(5.71%); N(17.03%); IR [(KBr) ν_{max}/cm^{-1}]: 3152, 2923, 2848, 1619, 1529, 1158, 1094, 928, 841, 731; solid-state ^{13}C NMR (δ ppm): 217, 163 and 150–120, 27; λ_{max} (solid state) (nm): 492 s, 599, 665 s, 767.

2.4.2. 2,9,16,23-tetra-{2-nonyl-[1,3,4]oxadiazole}-nickelphthalocyanine (3b). Yield: 90% (1.21 g); Anal. Calcd for $C_{76}H_{88}N_{16}NiO_4$: C(67.70%); H(6.58%); N(16.62%). Found: C(65.94%); H(5.47%); N(15.00%); IR [(KBr) ν_{max}/cm^{-1}]: 3177, 2921, 2851, 1612, 1526, 1144, 1090, 927, 840, 729; solid-state ^{13}C NMR (δ ppm): 219, 165, 150–120, 28; λ_{max} (solid state) (nm): 492 s, 599, 667 s, 767.

2.4.3. 2,9,16,23-tetra-{2-undecyl-[1,3,4]oxadiazole}-nickelphthalocyanine (3c). Yield: 87% (1.27 g); Anal. Calcd for $C_{84}H_{104}Cl_4N_{16}NiO_4$: C(69.08%); H(7.18%); N(15.34%). Found: $C_{64}H_{28}N_{16}Cl_4NiO_4$: C(67.98%); H(6.31%); N(14.10%); IR [(KBr) ν_{max}/cm^{-1}]: 3152, 2923, 2853, 1608, 1526, 1145, 1089, 927, 839, 729; solid-state ^{13}C NMR (δ ppm): 217, 165, 150–120, 30; λ_{max} (solid state) (nm): 477 s, 599, 668 s, 767.

2.4.4. 2,9,16,23-tetra-{2-tridecyl-[1,3,4]oxadiazole}-nickelphthalocyanine (3d). Yield: 82% (1.28 g); Anal. Calcd for $C_{92}H_{120}N_{16}NiO_4$: C(70.26%); H(7.69%); N(14.25%). Found: $C_{64}H_{28}N_{20}NiO_{12}$: C(70.1%); H(6.93%); N(13.37%); IR [(KBr) ν_{max}/cm^{-1}]: 3168, 2924, 2854, 1611, 1527, 1323, 1146, 1089, 928, 842, 730; solid-state ^{13}C NMR (δ ppm): 220, 163, 150–120, 28, 14; λ_{max} (solid state) (nm): 477 s, 597, 679 s, 778.

2.4.5. 2,9,16,23-tetra-{2-pentadecyl-[1,3,4]oxadiazole}-nickelphthalocyanine (3e). Yield: 76% (1.27 g); Anal. Calcd for $C_{100}H_{136}N_{16}NiO_4$: C(71.28%); H(8.14%); N(13.30%). Found: $C_{64}H_{28}N_{20}NiO_{12}$: C(70.11%); H(7.52%); N(12.21%); IR [(KBr) ν_{max}/cm^{-1}]: 3180, 2923, 2853, 1617, 1527, 1323, 1147, 1093, 927, 842, 731; solid-state ^{13}C NMR (δ ppm): 218, 163, 150–120, 29; λ_{max} (solid state) (nm): 477 s, 597, 679 s, 778.

2.4.6. 2,9,16,23-tetra-{2-heptadecyl-[1,3,4]oxadiazole}-nickelphthalocyanine (3f). Yield: 75% (1.34 g); Anal. Calcd for $C_{108}H_{152}N_{16}NiO_4$: C(72.18%); H(8.52%); N(12.47%). Found: $C_{64}H_{28}N_{20}NiO_{12}$: C(70.91%); H(7.21%); N(11.03%); IR [(KBr) ν_{max}/cm^{-1}]: 3196, 2922, 2852, 1616, 1527, 1322, 1147, 1092, 926, 841, 730; solid-state ^{13}C NMR (δ ppm): 219, 163, 150–120, 26, 13; λ_{max} (solid state) (nm): 477 s, 597, 679 s, 778.

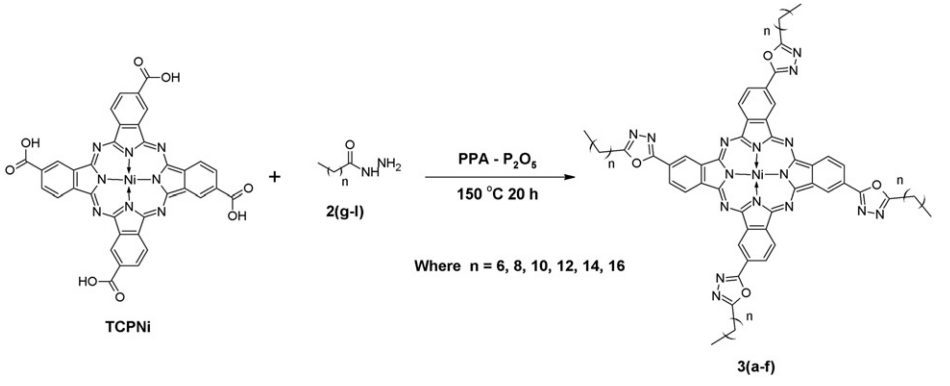

Scheme 1. Synthesis of tetraalkyl-[1,3,4]-oxadiazole-substituted NiPc.

3. Results and discussion

3.1. *Synthesis*

The target 2,9,16,23-tetra-alkyl-[1,3,4]-oxadiazole-substituted NiPcs **3a–3f** were obtained in good yield through melt condensation of **TCPNi** with fatty acid hydrazides of varying chain length **2g–2l** in the presence of PPA as a solvent and condensing agent (scheme 1).

Evidence for the formation of oxadiazoles with alkyl chain was provided by FT-IR, solid-state ^{13}C NMR, and electronic absorption spectroscopy.

3.2. *IR absorption spectra*

FT-IR spectra for NiPcs **3a–3f** exhibited a series of absorptions at 729–737, 839–847, 926–928, 1088–1093, and 1145–1148 cm^{-1}, which can be attributed to the Pc skeleton. The presence of peaks at 1608–1617 and 1527–1544 cm^{-1} for NiPcs **3a–3f** can be assigned to aromatic –C = N– and –C = C– in plane skeletal vibrations of the Pc core, respectively. Peaks at 3167–3190 cm^{-1} are associated with aromatic –C–H stretching vibrations and in the region 1089–1093 cm^{-1} is due to aromatic –C–H bending vibrations. However, the comparison of FT-IR spectra of **TCPNi** and NiPcs **3a–3f** reveals some marked differences, the characteristic absorptions due to –C = O of –COOH groups in **1** at 1697 cm^{-1} has disappeared in the IR spectra of NiPcs **3a–3f** indicating the involvement of carbonyl carbon in the formation of the oxadiazole. The two intense bands at 2924–2923 cm^{-1} for **3a–3f** were assigned for aliphatic –CH asymmetric and symmetric stretches. Characteristic stretching vibrations due to –C=N and –C–O– of the oxadiazole ring in **3a–3f** are coupled with coupled skeletal vibrations of –C=N– and –C=C– of the Pc core (figures S1 and S2, see Supplementary material).

3.3. *Solid-state ^{13}C NMR spectra*

Solid-state ^{13}C NMR spectra of the six tetra alkyl-[1,3,4]-oxadiazole-substituted NiPcs **3a–3f** at room temperature exhibited the expected broad signal at 120–150 ppm and an

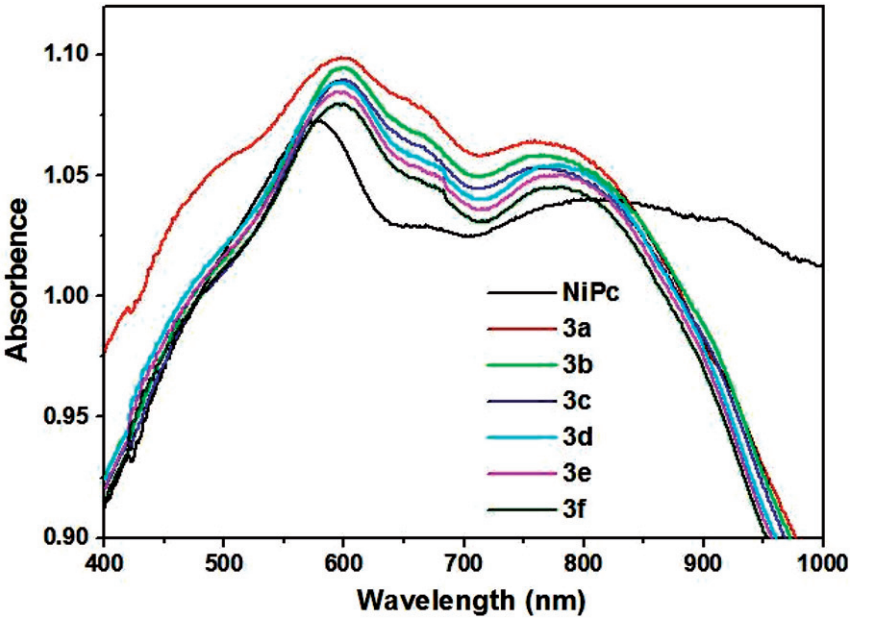

Figure 2. Solid-state electronic absorption spectra of **1** and **3a–3f**.

Table 1. Solid-state electronic absorption data for NiPc and **3a–3f**.

NiPc	Peaks λ_{max} (nm)
NiPc	577
3a	492s, 599, 665s, 767
3b	492s, 599, 667s, 767
3c	477s, 599, 668s, 767
3d	477s, 597, 679s, 778
3e	477s, 597, 679s, 778
3f	477s, 597, 679s, 778

additional peak at 162–167 ppm for aromatic carbons and aromatic carbons attached to nitrogen, respectively, for each compound. Peaks at 213–220 ppm were assigned to carbons attached to the electron-deficient oxadiazole in the NiPcs **3a–3f**. Further, the peaks at 13–30 ppm were assigned to aliphatic carbons in NiPcs **3a–3f** (figures S3 and S4, see Supplementary material).

3.4. *Electronic absorption spectra*

With peripheral alkyl oxadiazole-substituted Pc and some of its analogues at hand, the optical properties of these molecules were of considerable interest. Marked difference is apparent in representative solid-state electronic absorption spectrum shown in figure 2; results are summarized in table 1. The electronic spectra recorded from **3a** to **3f** in the solid state exhibit characteristic Q band at $\lambda \approx 600$ nm and a second band of lower

Table 2. Optical band gap data for NiPc and **3a–3f**.

NiPc	Peaks λ_{max} (nm)	Band gap (eV)
NiPc	577	2.043
3a	599	2.004
	767	1.410
3b	599	2.004
	767	1.410
3c	599	2.004
	767	1.410
3d	597	2.014
	778	1.458
3e	597	2.014
	778	1.458
3f	597	2.014
	778	1.458

intensity in the near IR region at $\lambda \approx 780$ nm. Splitting of Q band can be observed in **3a–3f** due a_{2u} to e_g and b_{2u} to e_g transitions, indicating effective electronic communication between the Pc core and the oxadiazole [36]. The chain length has hardly any influence on the position of the Q-band in NiPcs **3a–3f**, in agreement with previous work of Sleven *et al.* [37].

Further, the optical band gaps for oxadiazole-substituted Nipcs were determined by the absorption edge of the absorption spectrum of each compound in the solid state, and the data are summarized in table 2.

The presence of alkyl oxadiazole moieties into the NiPc core resulted in fine-tuning of the position of the Q-band and the alkyl oxadiazole-substituted NiPcs absorb a large part of the visible light region from 400 to 800 nm.

3.5. *Scanning electron microscopy*

Information on the morphology of the synthesized compounds was obtained from scanning electron microscopy (SEM) analysis. As revealed by SEM micrographs, alkyl oxadiazole-substituted NiPcs, **3a–3f**, particulates are not uniform in shape (figure 3). In all cases, the diameters of particulates are relatively uniform from 200 to 5000 nm. NiPc attached to the alkyl oxadiazole moiety can act as a nucleation center, further inducing growth of Pc crystallite. On close examination of the SEM images, with increase in alkyl chain length, the particle size decreased which can be accounted for by restricted accessibility of adjacent Pc molecules.

3.6. *Thermal analysis*

Thermal analyses of the complexes were recorded in air from 29°C to 600°C. Analysis of thermogravimetric curves and the corresponding data reveal that it is difficult to find demarcation between the steps of loss of peripheral substitution and the destruction of the Pc core. The residues after thermal decomposition are around 7–10% corresponding to metal oxide.

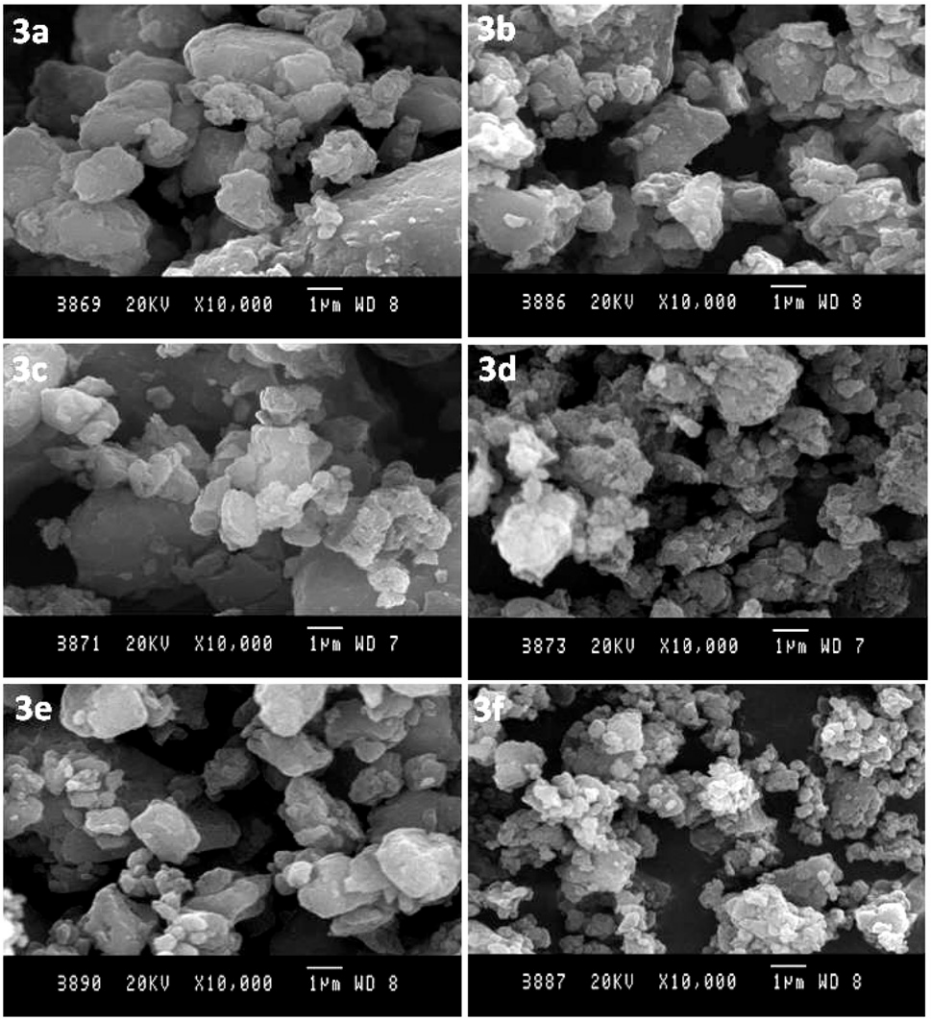

Figure 3. SEM micrographs for NiPc **3a–3f**.

Kinetic and thermodynamic parameters were computed using Broido's method [38]. The plots of $\ln(\ln 1/Y)$ *versus* $1/T$ (where Y is the fraction of the compound undecomposed) were developed for decomposition (figure S6, see Supplementary material). From the plots the thermoanalytical data and activation properties, such as energy of activation (E_a), frequency factor ($\ln A$), enthalpy ($\Delta H^{\#}$), entropy ($\Delta S^{\#}$), and free energy ($\Delta G^{\#}$), were evaluated (table S1, see Supplementary material).

3.7. *XRD studies*

The powdered XRD pattern of alkyl-[1,3,4]-oxadiazole-substituted NiPcs **3a–3f** are presented in figure S7 (see Supplementary material). It is evident from the diffraction

pattern that the alkyl oxadiazole-substituted Pcs exhibit identical broad peaks with diffused intensity, but the peak intensity gradually increased with increase in chain length.

The presence of electron-deficient hetero aromatic oxadiazole in the Pc periphery results in extended conjugation and influences the stacking arrangements of the Pcs with the nickel in parallel molecules, increasing the orbital overlap between parallel pairs of molecules. Data of 2θ, lattice spacing, and relative intensity are provided in supporting information (table S2, see Supplementary material).

3.8. *DC electrical conductivity studies*

The magnitude of room temperature DC electrical conductivity observed for NiPcs **3a–3f** are $\sim 10^3$ times higher compared to parent NiPc [39]. The room temperature DC electrical conductivities of tetraalkyl oxadiazole-substituted NiPcs is **3a** > **3b** > **3c** > **3d** > **3e** > **3f**. This decrease in conductivity from **3a** to **3f** can be ascribed to decrease in intermolecular interaction with increase in chain length. The temperature dependence of conductivity can be expressed as

$$\sigma = \sigma_0 \exp\left[\frac{-\Delta E}{kT}\right],$$

where σ is DC electrical conductivity at temperature T, σ_0 is the pre-exponential factor, k is Boltzmann's constant, and ΔE is the activation energy.

Figure 4(a) shows the variation of resistivity with temperature. For **3a–3f**, the resistivity decreases with increase in temperature. Further, figure 4(b) represents Arrhenius plots of log σ_{DC} (DC conductivity) *versus* $1/T$ (reciprocal of temperature) for **3a–3f** from 300 to 500 K. The thermal activation energies (ΔE) obtained from Arrhenius plots, collected in table 3, are considerably less than the parent NiPc [39]. The plots reveal that the temperature has pronounced effect on DC conductivity and all the new Pc molecules are semiconducting. The increase in DC electrical conductivity of NiPcs **3a–3f** with increase in temperature can be explained; in that conduction occurs by electron transfer across insulating gaps in the conducting pathway by fluctuation-induced tunneling proposed by Sheng [40] and hopping at the localized states in the amorphous regions between the small metallic regions [41].

4. Conclusion

Melt condensation of **TCPNi** with alkyl acid hydrazides resulted in the formation of alkyl-[1,3,4]-oxadiazole NiPcs **3a–3f** in good yield. The solid-state electronic absorption spectra of **3a–3f** indicate effective electronic communication between the Pc core and the oxadiazole. Introduction of an alkyl-[1,3,4]-oxadiazole group on the periphery of an NiPc strongly affects the spectroscopic properties of the Pc resulting in splitting of the Q-band and appearance of an additional band of low intensity in the near IR region; chain length has hardly any influence on the position of the Q-band in **3a–3f**. The room temperature DC electrical conductivities observed for **3a–3f** are $\sim 10^3$ times higher than the parent NiPc and increase with increase in temperature with significant

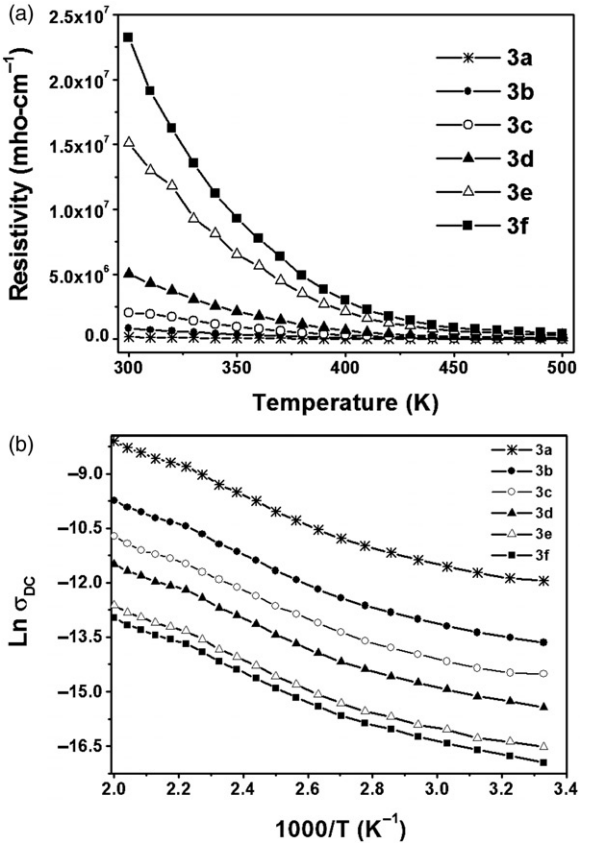

Figure 4. (a) Variation of resistivity with temperature for **3a–3f**; (b) Arrhenius plots for **3a–3f**.

Table 3. Activation energy for NiPcs **3a–3f**.

NiPc	Conductivity σ_{DC} at 300 K (mho cm^{-1})	ΔE (300–500 K) (eV)
3a	6.52×10^{-6}	0.083
3b	1.18×10^{-6}	0.088
3c	4.97×10^{-7}	0.099
3d	1.98×10^{-7}	0.100
3e	6.61×10^{-8}	0.102
3f	4.31×10^{-8}	0.107

decrease in thermal activation energy. DC electrical conductivities for alkyl-[1,3,4]-oxadiazole-substituted NiPcs decrease with increase in chain length at the Pc periphery due to decrease in intermolecular interaction with increase in chain length. The new Pcs with considerable stability, excellent optical, and DC conductivity may be regarded as an important step in developing a viable sensor and semiconducting material.

Supplementary material

FT-IR spectra of **3d** and **3e** (figures S1 and S2), solid-state ^{13}C NMR spectrum of **3d** and **3f** (figures S3 and S4), probable stacking arrangements in NiPc **3a–3d** (figure S5), kinetics of thermal decomposition (table S1 and figure S6), powdered XRD pattern for **1** and **3a–3f** (figure S7), and powdered XRD data for NiPc and NiPcs **3a–3f** (table S2) are given in on-line Supplementary material.

Acknowledgments

The authors thank Prof. S. Natrajan, IISc, Bangalore, for providing solid-state electronic absorption spectra, as well as the NMR Research Center, IISc, Bangalore, for providing solid-state ^{13}C NMR spectra.

References

[1] C.C. Leznoff, A.B.P. Lever. *Phthalocyanines: Properties and Applications*, Vols. I–IV, V.C.H. Publications, New York (1986–1993).
[2] N.B. McKeown. *Phthalocyanine Materials – Synthesis Structure and Function*, Cambridge University Press, Cambridge (1998).
[3] K. Kadish, K.M. Smith, R. Guilard. *The Porphyrin Handbook*, Vols. 15–20, Academic Press, New York (2003).
[4] H.S. Nalwa. *Supramolecular Photosensitive and Electroactive Materials*, Academic Press, New York (2001).
[5] O.A. Osmanbas, A. Koca, I. Ozcesmeci, A.I. Okur, A. Gul. *Electrochim. Acta*, **53**, 4969 (2008).
[6] J. Yum, S. Jang, R. Humphry-Baker, M. Gratzel, J. Cid, T. Torres Md., K. Nazeeruddin. *Langmuir*, **24**, 5636 (2008).
[7] A. Schuetze, N. Pieper, J. Zacheja. *Sensors Actuators, B*, **23**, 215 (1995).
[8] G. de la Torre, P. Vazquez, F. Agullo-Lopez, T. Torres. *Chem. Rev.*, **104**, 3723 (2004).
[9] B.A. Minch, W. Xia, C.L. Donley, R.M. Hernandez, C. Carter, M.D. Carducci, A. Dawson, D.F. O'Brien, N.R. Armstrong. *Chem. Mater.*, **17**, 1618 (2005).
[10] F. Harnisch, N.A. Savastenko, F. Zhao, H. Steffen, V. Bruser, U. Schroder. *J. Power Sources*, **193**, 86 (2009).
[11] H. Shiokawa, M. Hiramoto. *Mol. Cryst. Liq. Cryst.*, **491**, 277 (2008).
[12] D. Guillon, A. Skoulios, C. Piechocki, J. Simon, P. Weber. *Mol. Cryst. Liq. Cryst.*, **100**, 275 (1983).
[13] P.G. Schouten, J.M. Warman, M.P. de Haas, M.A. Fox, H.L. Pan. *Nature*, **353**, 736 (1991).
[14] J.M. Warman, M.P. de Haas, J.F. van der Pol, W. Drenth. *Chem. Phys. Lett.*, **164**, 581 (1989).
[15] E. Orti, J.L. Bre'das, C. Clarisse. *J. Chem. Phys.*, **92**, 1228 (1990).
[16] J. Simon, P. Bassoul. *Phthalocyanines Properties and Applications*, Chap. 6, VCH, New York (1993).
[17] J.F. van der Pol, E. Neeleman, J.W. Zwikker, R.J.M. Nolte, W. Drenth, J. Aerts, R. Visser, S.J. Picken. *Liq. Cryst.*, **6**, 577 (1989).
[18] (a) H. Mukai, M. Yokokawa, K. Hatsusaka, K. Ohta. *J. Porphyrins Phthalocyanines*, **13**, 70 (2009); (b) U. Kumru, M.A. Ermeydan, F. Dumoulin, V. Ahsen. *J. Porphyrins Phthalocyanines*, **12**, 1090 (2008); (c) S.Y. Al-Raqa. *J. Porphyrins Phthalocyanines*, **10**, 55 (2006).
[19] H. Kantekin, M. Rakap, M.N. Misir, H.Z. Gok, I. Acar. *J. Coord. Chem.*, **60**, 1965 (2007).
[20] H. Kantekin, Y. Gok, M.B. Kilicaslan, I. Acar. *J. Coord. Chem.*, **61**, 229 (2009).
[21] M.K. Engel, P. Bassoul, L. Bosio, H. Lehmann, M. Hanack, J. Simon. *Liq. Cryst.*, **15**, 709 (1993).
[22] C.F. van Nostrum, A.W. Bosman, G.H. Gelinck, P.G. Schouten, J.M. Warman, A.P.M. Kentgens, M.A.C. Devillers, A. Meijerink, S.J. Picken, U. Sohling, A.J. Schouten, R.J.M. Nolte. *Chem. Eur. J.*, **1**, 171 (1995).
[23] J.M. Kroon, R.B.M. Koehorst, M. van Dijk, G.M. Sanders, E.J.R. Sudholter. *J. Mater. Chem.*, **7**, 615 (1997).
[24] G.J. Clarkson, A. Cook, N.R. McKeown, K.E. Treacher, Z. Ali-Adib. *Macromolecules*, **29**, 913 (1996).

[25] K. Hatsusaka, K. Ohta, I. Yamamoto, H. Shirai. *J. Mater. Chem.*, **11**, 423 (2001).
[26] P.G. Schouten, J.F. van der Pol, J.W. Zwikker, W. Drenth, S.J. Picken. *Mol. Cryst. Liq. Cryst.*, **195**, 291 (1991).
[27] M.N.K. Harish, J. Keshavayya, K.R. Venugopala Reddy, H.R. Mallikarjuna, R.A. Shoukat Ali, T. Rajesh. *J. Coord. Chem.*, **63**, 4050 (2010).
[28] C. Jiang, W. Yang, J. Peng, S. Xiao, Y. Cao. *Adv. Mater.*, **16**, 537 (2004).
[29] S. Tokito, M. Suzuki, F. Sato, M. Kamachi, K. Shirane. *Org. Electron.*, **4**, 105 (2003).
[30] C. Risko, E. Zojer, P. Brocorens, S.R. Marder, J.L. Bredas. *Chem. Phys.*, **313**, 151 (2005).
[31] S. Janietz, S. Anlauf, A. Wedel. *Macromol. Chem. Phys.*, **203**, 433 (2002).
[32] X. Zhan, Y. Liu, X. Wu, S. Wang, D. Zhu. *Macromolecules*, **35**, 2529 (2002).
[33] M. Ichikawa, T. Kawaguchi, K. Kobayashi, T. Miki, K. Furukawa, T. Koyama, Y. Taniguchi. *J. Mater. Chem.*, **16**, 221 (2006).
[34] Y.D. Zhang, K.G. Jespersen, M. Kempe, J.A. Kornfield, S. Barlow, B. Kippelen, S.R. Marder. *Langmuir*, **19**, 6534 (2003).
[35] X. Song, Y. She, H. Ji, Y. Zhang. *Org. Process Res. Dev.*, **9**, 297 (2005).
[36] D.M.P. Mingos (Series Ed.), Jianzhuang Jiang (Volume Ed.). In *Structure and Bonding*: *Functional Phthalocyanine Molecular Materials*, pp. 46–65, Springer-Verlag, Berlin, Heidelberg (2010).
[37] J. Sleven, T. Cardinaels, C. Gorller-Walrand, K. Binnemans. *ARKIVOC*, **iv**, 68 (2003).
[38] A. Broido. *J. Polym. Sci., Part A-2: Polym. Phys.*, **7**, 1761 (1969).
[39] M.M. EL-Nahass, A.F. EL-Deeb, F. Abd-El-Salam. *Org. Electron.*, **7**, 261 (2006).
[40] P. Sheng. *Phys. Rev. B*, **21**, 2180 (1980).
[41] Y.J. Wang, M.D. Newton, J.W. Davenport. *Phys. Rev. B*, **46**, 11935 (1992).